Global Scientific JOURNALS

GSJ: Volume 8, Issue 7, July 2020, Online: ISSN 2320-9186
www.globalscientificjournal.com

Numerical Investigation Of Two-Phase Laminar Pulsating Nanofluid Flow In AnInterruptedMicrochannel Heat Sink

Ayodeji S. Binuyo.

Department of Mechanical Engineering, Obafemi Awolowo University, Ile-Ife, Nigeria.E-mail: binuyoayodeji@gmail.com

KeyWords

Interrupted microchannel, rectangular rib, nanofluid, nanoparticle volume fraction, Pulsating flow, Dimessionless amplitude, Nusselt number, Reynolds number.

ABSTRACT

This study numerically investiagates the heat transfer characteristics ofAl_2O_3-water-based nanofluids in a a three-dimensional interrupted microchannel heat sink with rectangular ribs (IMCHS-R) under pulsating inlet flow conditions.The two-phase mixture model with modified effective thermal conductivity and viscosity equations is used to solve the problem numerically.While nanoparticle volume fraction and other parameters are kept constant, the effect ofdifferent values of Reynolds numbers (200-1000), pulsating frequencies(100-500Hz) and amplitudes (0.2-0.8) on the rate of heat transferwere examined. The results show that the rate of heat transfer improves significantly for sinusoidal velocity inlet conditions compared with steady flow conditions.

1 Introduction.

Thermal management is a critical factor to be considered in the development of electronic systems due to the challenges posed by the of high heat flux encountered in these systems. After Tuckerman and Pease[1] pioneered the investigation related to the use of microchannel heat sink (MCHS) for coolingpurpose and discovered its ability to dissipate a large amount of heat from the high density very-large-scale integrated circuit (VLSI), numerous research works have been carried out to further improve the performance characteristics of such devices. Peng and Peterson [2] carried out an experimental investigation on single phase forced convective heat transfer and flow characteristic in a rectangular microchannel heat sink with water as working fluid. Based on their result, they concluded that the geometry of the microchannel played a major role in determining the heat transfer and fluid flow characteristics.They then propose an empirical correlation for the Nusselt number and friction factor for laminar, transition and turbulent flow. Harms et al [3] conducted an experimental study on developing flow of convective heat transfer in deep rectangular microchannel using Deionized water as the working fluidfor Reynolds number within the range of 173 to 12900, their results indicate that microchannel systems designed for developing laminar flow performed better than those designed for turbulent flow. Qu and Mudawar [4] experimentally and numerically studied the pressure drop and heat transfer characteristic in a single-phase water-cooled microchannel heat sink of height and depth of 231μm and 713 μm respectively. Based on their result, they concluded that that for Reynolds number within the range of 132 to 1672, there is no rapid transition from laminar to turbulence flow, pressure drop depends on the operating Reynolds number, water viscosity depends on its temperature and that the temperature distribution of experimental data was in decent agreement with numerical predictions.Ambatipudi and Rahman [5] numerically examined the heat transfer through a silicon microchannel. The result showed that the for the design with greater number of channel and higher Reynolds number, higher Nusselt number was obtained. Numerous experimental and numerical studies [6-12] conducted in the past have contributed immersely to the advancement of MCHS and in understanding of its heat transfer and flow characteristics.

Since the interruption of boundary layer and provison of more surface area with the use of passive structures improves macro scale heat transfer. In case of micro scale heat transfer, several studies [13-18] in the past reveal that interruption of boundary layer and induced main stream separation are two significant means of enhancing heat tranfer in the micro scale. Therefore, microchannel with passive structures provides a better heat transfer performance than the smooth microchannel. Chai et al [19] performed numerical analysis on the Optimal thermal design of interrupted microchannel heat sink with rectangular ribs in transverse microchambers, numerical result showed that for heat transfer enhancement, the interrupted microchannel with ribs is suitable to the operating condition of $Re < 600$, and for $Re > 600$, the interrupted microchannel without ribs is considered better. Also, the new interrupted microchannel with rectangular rib length of 0.5 mm provides the highest enhancement factor.

The nanofluids are modern heat transfer fluids, they consist of a base fluid stably suspended with nanoparticles (average size below 100 nm). Several numerical and experimental studies [20-23] were performed on the use of nanofluid to enhance the heat transfer. It has been observed that nanofluidsexhibit excellent heat transfer capabilities compared with conventional heat transfer fluids and that thermal enhancement increases on increasing the nanoparticle concentration.Lotfi et al [24]studied the forced convective heat transfer of nanofluid flow through horizontal circular tube. The objective of the study was to investigate the accurateness of the single-phase model, two-phase mixture model and two-phase Eulerian model against previous experimental work. It was concluded that the mixture model provided better results as compared to all the other models.Kalteh et al [25] numerically and experimentally studied the laminar convective heat transfer of Al_2O_3-H_2O nanofluid flow through a wide rectangular MCHS. The two-phase Eulerian–Eulerian model was adopted for the numerical study. It was proven that the two-phase numerical results were in good agreement with experimental results as compared to single-phase results with maximum error of 7.42% and 12.61%.

Nandi and Chattopadhyay [26] carried out a numerical study to investigate simultaneously developing laminar fluid flow and heat transfer inside a two-dimensional wavy wall microchannel under pulsating inlet flow condition. It was found that with pressure drop within the acceptable limits the pulsating velocity can enhance heat transfer performance when compared with equivalent steady case.Akdag et al. [27] performed a numerical investigation with the same geometry and parameters with Nandi and Chattopadhyay [26]. They further the research by introducing Al_2O_3–water based nanofluids via the single-phase approach. they observed an increase in heat transfer performance on increasing nanoparticle volume fraction and amplitude of pulsation.Akdag et al. [28] numerically investigated the heat transfer characteristics of CuO-water-based nanofluids in a trapezoidal-corrugated channel under pulsating inlet flow conditions, it was found that the use of nanoparticles under the pulsating flow conditions increases the heat transfer rate compared with the steady flow case.Narrein et al [29]investigateda three dimentionaltwo-phase laminar pulsating nanofluid flow in a helical microchannel.The two-phase mixture model with modified effective thermal conductivity and viscosity equations is employed to solve the problem numerically. Detailed numerical results showed that an increase inpulsation frequency lead to a significant increase in rate of heat transfer when compared to pulsation amplitude. Also, increase in nanoparticle volume concentration lead to a decrease in nusselt number due to increase in nanofluid thermal conductivity.

Literature survey showed that few studies have investigated pulsating nanofluids flow in microchannels. But no comprehensive study in the pasthas been made to investigate the heat transfer and flow characteristics of pulsating nanofluid in aninterrupted mcrochannel heat sink with rectangular ribs (IMCHS-R) using two-phase mixture model.Hence, this has motivated the present study which examines the three-dimensional unsteady laminar flow of Al_2O_3 nanofluids in an IMCHS-R with the effects of different amplitude (0.2–0.8), frequency (100–500 Hz), and Renolds number (200-1000) at a constant nanoparticle concentration (1%).

2. Mathmatical Model.

2.1 Description of physical and computational domain

Figure 1 shows the basic geometry of the interrupted microchannel heat sink used in the present study. The geometry is based on the result of chai et al [13].To save the computation time and take advantage of symmetry, a control volume containing a single microchannel and surrounding solid along with the base is selected for developing the fluid flow and heat transfer model as shown in Figure 2. The dimensions of geometric parameters in the figure 1 and figure 2 is shown in Table 1.

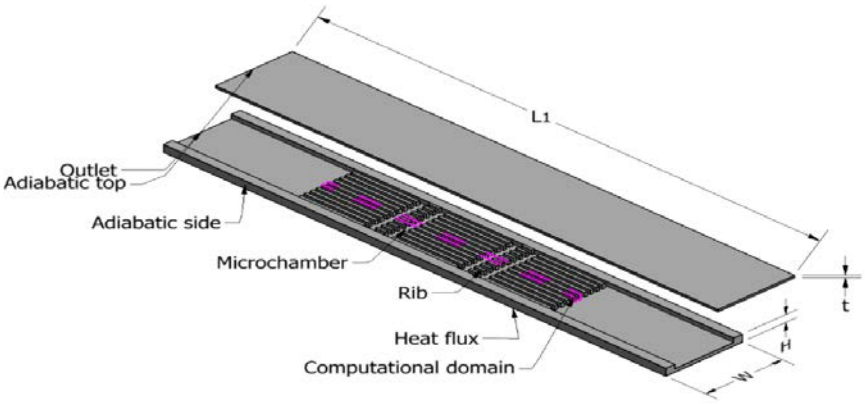

Figure 1: Interrupted Microchannel Heat Sink

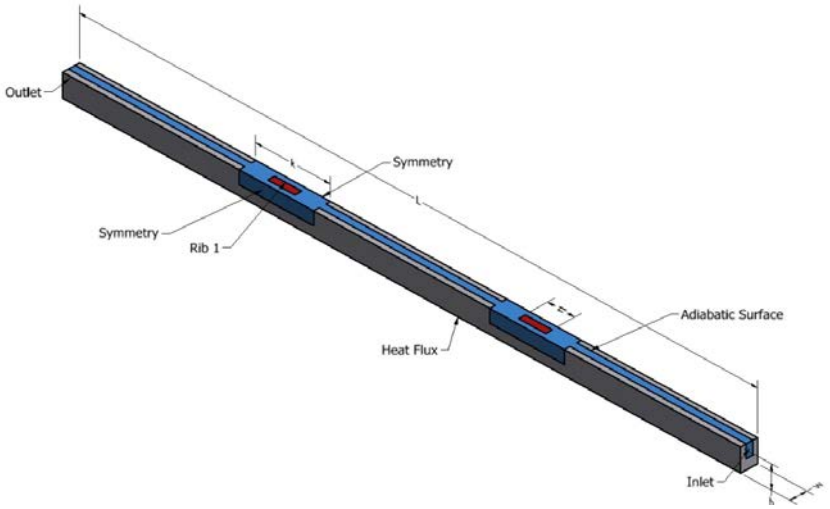

Figure 2: Computational domain of the interrupted microchannel heat sink (IMCH-R)

Table 1: Dimension of the Microchannel heat sink

Parameter	Dimension
L(a)	20mm
W	2.5mm
h	0.35mm
T	0.1mm
L(b)	10mm
K	1.1mm
r1	0.4mm
w	0.25mm
H	0.35mm

2.2 Governing Equations

Since heat is transferred from the base wall of the microchannel heat sink to the nanofluid which flows through the channel. Several assumptions are made on the operating conditions of the microchannel heat sink as follows:

(i) Developing flow and heat transfer in microchannels
(ii) The flow in the microchannel heat sink is steady and laminar
(iii) Temperature dependent thermal-physical properties of nanofluid
(iv) The properties of the microchannel heat sink material are temperature independent
(v) The external heat transfer effects are ignored.

The mixture model can model phases (fluid or particulate) by solving the momentum, continuity, and energy equations for the mixture, the volume fraction equations for the secondary phases, and algebraic expressions for the relative velocities.
According to the ANSYS fluent theory guide [30], the governing equations of the mixture model can be written as shown below.
Continuity equation:

$$\frac{\partial}{\partial t}(\rho_m) + \nabla.\left(\rho_m \vec{V}_m\right) = 0 \quad (1)$$

Where,

$$\rho_m = \sum_{k=1}^{n} \alpha_k \rho_k$$

Momentum balance:

$$\frac{\partial}{\partial t}\left(\rho_m \vec{V}_m\right) + \nabla.\left(\rho_m \vec{V}_m \vec{V}_m\right) = -\nabla p + \nabla.\left[\mu_m \left(\nabla \vec{V}_m + \nabla \vec{V}_m{}^T\right)\right] + \rho_m \vec{g} + \vec{F} - \nabla.\left(\sum_{k=1}^{n} \alpha_k \rho_k \vec{V}_{dr,k}\, \vec{V}_{dr,k}\right) \quad (2)$$

where n is the number of phases, $\vec{F}$ is a body force, and μ_m is the viscosity of the mixture

$$\mu_m = \sum_{k=1}^{n} \alpha_k \mu_k \quad (3)$$

$\vec{V}_{dr,k}$ is the drift velocity for secondary phase *k*

$$\vec{V}_{dr,k} = \vec{V}_k - \vec{V}_m$$

Energy equation:

$$\frac{\partial}{\partial t}\left(\sum_{k=1}^{n} \alpha_k \rho_k E_k\right) + \nabla.\left[\sum_{k=1}^{n} \alpha_k \vec{V}_k (\rho_k E_k + p)\right] = \nabla.\left[\mathrm{k}_{eff} \nabla \mathrm{T}\right] + \mathrm{S_E} \quad (4)$$

where k_{eff} is the effective conductivity, the first term on the right-hand side of equation represents energy transfer due to conduction and $\mathrm{S_E}$ represent any other volumetric heating force.

2.3 Boundary conditions

A uniform heat flux of $1.22\mathrm{M}\ W/m^2$ is imposed at the silicon substrate bottom wall of the microchannel. The temperature at the inlet of the microchannel is taken to be 293 K. The external walls are assumed adiabatic with no convection or radiation heat transfer with the surrounding environment. The nanofluid enters the inlet with a transient velocity and exits the outlet at the atmospheric pressure. On all the conjugate surfaces, a no-slip boundary condition is imposed.the inlet velocity profile is given by:

$$\mathrm{U_{in}} = \mathrm{U_{ave}}\left[1 + \mathrm{A}\sin(2\pi \mathrm{ft})\right] \quad (5)$$

Where $\mathrm{U_{ave}}$ is the average velocity in the constant cross section region, A is the dimensionless amplitude of pulsation and f is the pulsating frequency in (Hz).

2.4 Physical Properties of Nanofluid

The density and specific heat capacity of nanofluid are defined as [31]:

$$\rho_{nf} = (1-\varphi)\rho_f + \varphi\rho_p \quad (6)$$

$$(\rho c_p)_{nf} = (1-\varphi)(\rho c_p)_f + \varphi(\rho c_p)_p \quad (7)$$

The effective thermal conductivity (k_{eff}) of the nanofluid is defined as [32]:

$K_{eff} = K_{static} + K_{dynamic}$

Where:

$$k_{static} = k_f\left\{\frac{(k_p+2k_f)-2\varphi(k_f-k_p)}{(k_p+2k_f)+\varphi(k_f-k_p)}\right\} \quad (8)$$

$$K_{dynamic} = 5*10^4\varphi\rho_f Cp_f\sqrt{\frac{K_bT}{d_p\rho_p}}\,g(T,\alpha) \quad (9)$$

The "g function" ($g(T,\alpha)$) in the equation above is given as:

$$g(T,\alpha) = (a + bln(dp) + cln(\alpha) + dln(\alpha)\ln(\mathrm{dp}) + \mathrm{eln}(dp)^2)\ln(T) + (m + hln(dp) + iln(\alpha) + jln(\alpha)\ln(\mathrm{dp}) + \mathrm{kln}(dp)^2) \quad (10)$$

The value of the constants in the above equation has been determined semi-empirically and are given in Table 2.

Table 2: The g-function constant values.

Constant	Values
A	52.81348876
B	6.115637295
C	0.695574508
D	4.17E-02
E	0.1769193
M	-298.1981908
H	-34.53271691
I	-3.922528928
J	-0.235432963
K	-0.999063481

The effective viscousity (μ_{eff}) of the nanofluid isdefined:

$\mu_{eff} = \mu_{static} + \mu_{dynamic}$

where the static part [33] and dynamic part are respectively defined as follows:

$$\mu_{static} = \frac{\mu_f}{(1-\alpha)^{2.5}} \quad (11)$$

$$\mu_{dynamic} = 5*10^4\alpha\rho_f\sqrt{\frac{K_bT}{d_p\rho_p}}\,g(T,\alpha) \quad (12)$$

Where the subscripts f, p and nfrepresent basefluid, nano particles and nanofluids respectively. Also,α and d_p represent nano particle concentration and diameter respectively.

The thermo-physical properties of pure water aredefinedas [34,35]:

$$\mathrm{k}_f = 0.6(1 + 4.167\times10^{-5}T) \quad (13)$$

$\mu_f = 2.761 \times 10^{-6} \exp(1713/T)$(14)

2.4 Numerical Procedures

The numerical computations of this study are carried out by solving the governing equations with associated boundary conditions using the finite-volume method. The pressure and the velocity fields were coupled using the SIMPLEC algorithm. The second-order upwind differencing scheme is selected for the convective terms. The accuracy of the solution to convergence was monitored at 10^{-6} for the continuity, velocity and $2e^{-8}$ for the energy equation.Eqs. (7)– (13) are used for redefining the effective thermal conductivity and viscosity because conventional equation used in the two-phase mixture model overpredicts the thermal conductivity, while a viscosity value is also required for the second phase. Numerical simulation is carried out for different combinations of Renolds number, amplitude, frequency, while nanoparticle concentration and other parametrs are kept constant. As shown is Eq. (20), the inlet velocity, $\mathrm{U_{in}}$, varies periodically about an equilibrium value,$\mathrm{U_{ave}}$, based on the specified amplitude and frequency. A full period of oscillation is considered in the inlet velocity and the maximum number of iterations per time step is set to 2000. This value is chosen based upon the fact that 1000–1,800 iterations are needed per time step for the flow and thermal field results to reach steady state.

2.5Data Acquisition

To present the numerical results of heat transfer and flow characteristics for the present analysis, the following important parameters are given below according to chai et al [19]:

Reynolds number:

$Re = \frac{\rho_{nf} \mathrm{V}_{avg} D_h}{\mu_{nf}}$ (15)

Where ρ_{nf} is the volume average nanofluidfluids density (kgm^{-3}), D_h is the hydraulic diameter calculated based on the constant cross-section region (m), μ_{nf} is the mass average nanofluids dynamic viscosity ($kg\ m^{-1}\ s^{-1}$) and V_{avg} is the average velocity in the constant cross-section region ($m\ s^{-1}$).

Time averaged heat transfer coefficient and Nusselt number for pulsating flow is defined as:

$h = \frac{1}{\tau L} \int_0^L \int_0^\tau h(x,t)\, dx\, dt$(16)

$Nu = \frac{1}{\tau L} \int_0^L \int_0^\tau Nu(x,t)\, dx\, dt$(17)

Average heat transfer coefficient and Nusselt number:

$\bar{h} = \frac{q_w LW}{A(\bar{T}w - \bar{T}f)}$(18)

$\bar{N}u = \frac{\bar{h} D_h}{k_f}$(19)

Where $\bar{T}w$ and$\bar{T}f$ are the area-weighted temperature of the silicon base and the mass-average temperature of nanofluids in themicrochannel.q_w represents heat flux at the silicon base, A is the contact surface area of water andsilicon based on the smooth microchannel, L and W are respectively the length and width of the computational domain, k_{nf} is the mass average nanofluidfluidsthermal conductivity.

The average Fanning friction factor is given by:

$f_{ave} = \frac{(\mathrm{p}_{in} - \mathrm{p}_{out}) D_h}{2\rho_f L u_m^2}$(20)

Where p_{in} is the mass-weighted average pressure in the microchannel inlet, L is the length of the interrupted microchannel heat sink, p_{out} is the time averaged pressure in the microchannel outlet and assumed to be 0.

3 Model Verification and Validation

3.1Grid Independence Analysis

The aim of grid independence analysis is to evaluate the effects of grid sizes on the numerical results. To test grid independence of the present study, different mesh sizes was generated using ANSYS design modeler. Hexagonal mesh of 0.35 million, 0.55 million, 0.75 million, 0.95million and 1.15 millioncells are considered.The inlet temperature of the channel is set to 293 K with a velocity of 5 m/s. A constant heat flux of$1.22\mathrm{M}\ W/m^2$is imposed at the silicon substrate bottom wall of the microchannel.The percentage difference of Nusselt number using 0.35, 0.55, 0.75 and 0.95 million cells from that of 1.15 million cells are 9.56%, 5.68%, 1.57 % and 1.55% respectively. Thus, we use a domain with approximately 0.75 million cells for all other cases to reduce the computing time.

3.2 Model Validation

The code validation for the Interrupted microchannel heat sink with rectangular ribs (IMCS-R) is performed based on thefindings presented by Chaiet al[19].It can be seen from Figure 3that the that maximum deviation of numerical f_{ave} from experimental results is less than 3%.The results for the two-phase mixture model of the present study is validated by comparing the results obtained for a nanoparticle volume fraction of ϕ = 1% and 500 ≤ *Re* ≤ 2000 with the numerical results of Lotfi et al. [25] and experimental result of Weng and Ding [36]. It can be seen from figure 4 that the results of present analysisare in excellent agreement with the experimental and numerical results of previous studies.

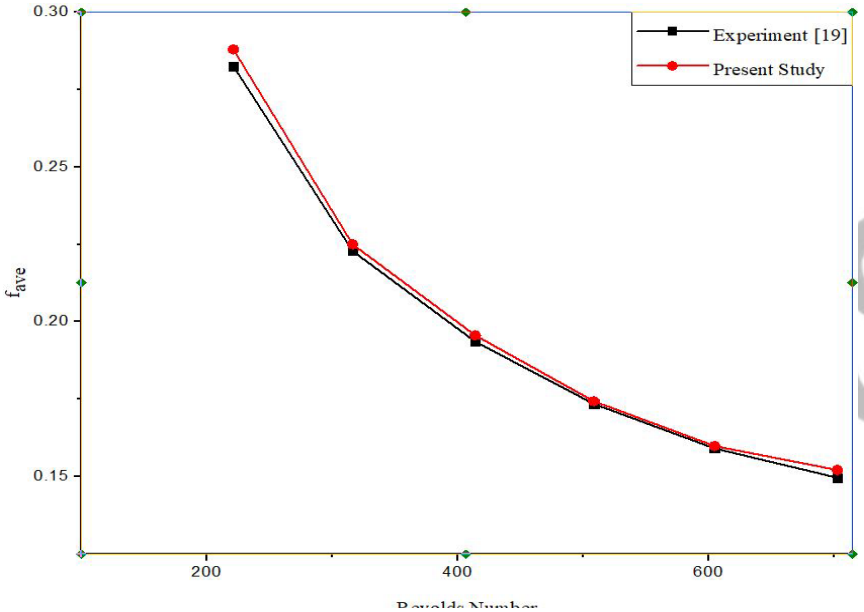

Figure 3: Comparison of present numerical result with experimental data of Chai et al [19]

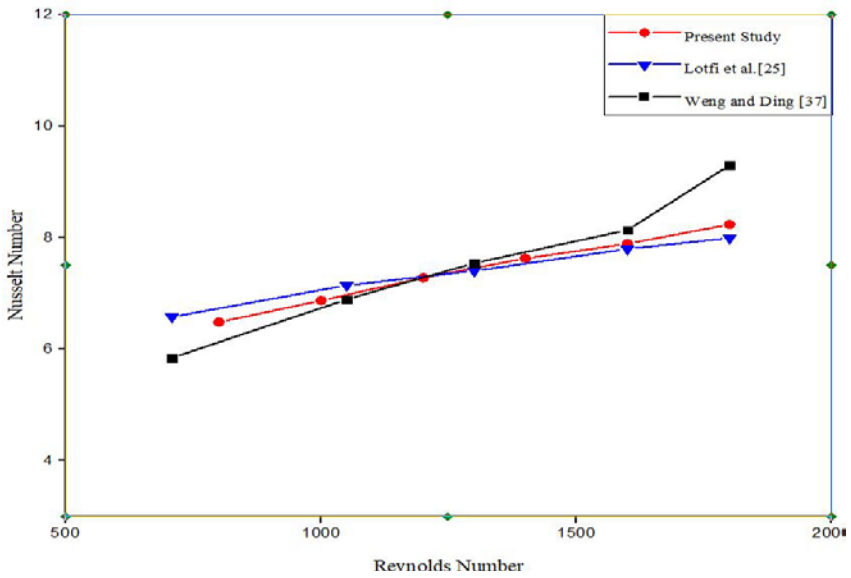

Figure 4: Comparison of present numerical result with past literatures

4 Results and Discussion

Figure 5a to 5c shows the comparison of time averaged Nu value between steady state and pulsating conditions for different amplitudes and constant frequency. It is observed for all cases that at lower Reynolds number there is a significant increase in the unsteady Nu value compared with steady Nu valuewhich is due to enhance mixing effect caused by introduction of pulsation into the flow domain. As Reynolds number increases there is an increase in Nu value for both steady and unsteady cases. Also, there is an increase in Nu values with increase in amplitude and frequency of pulsation. This shows that introduction of pulsation into the flow increases the rate of heat transfer when compared to steady case because it improves mixing process between the core and near wall fluid especially by predominating the viscous forces which is superimposed with the main flow [26]. It is also observed that the mixing effect as a result of pulsating amplitude diminishes at higher Reynold's number because the dominant effect of the secondary flow due to the presence of rectangular rib in the flow domain [19] suppresses the mixing effect caused by the inlet pulsating flow condition at higher Reynolds number.

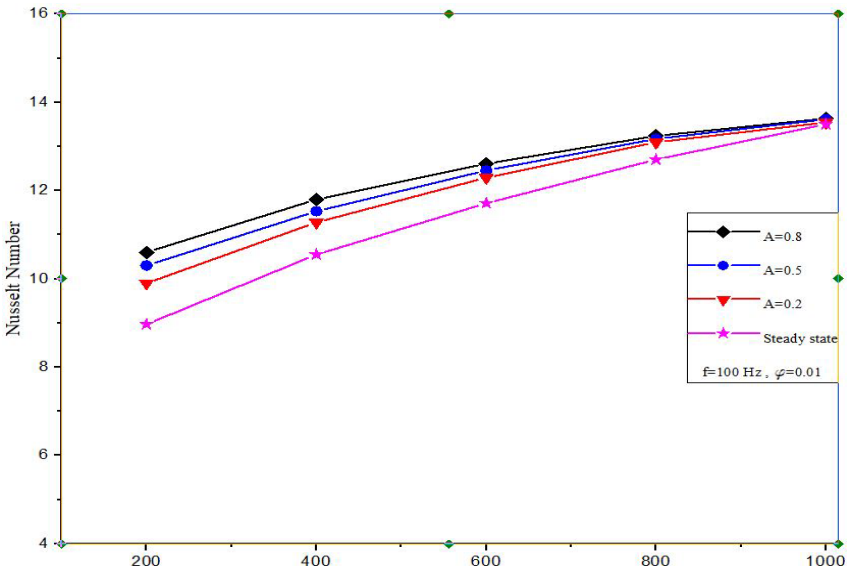

Figure 5a: Comparison of Nu values at various amplitudes and a frequency of 100Hz with steady state

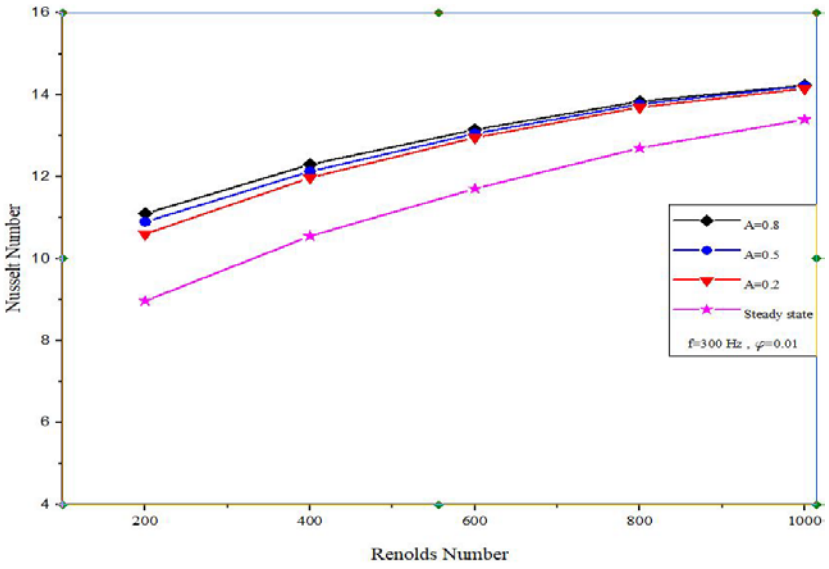

Figure 5b: Comparison of Nu values at various amplitudes and a frequency of 300Hz with steady state

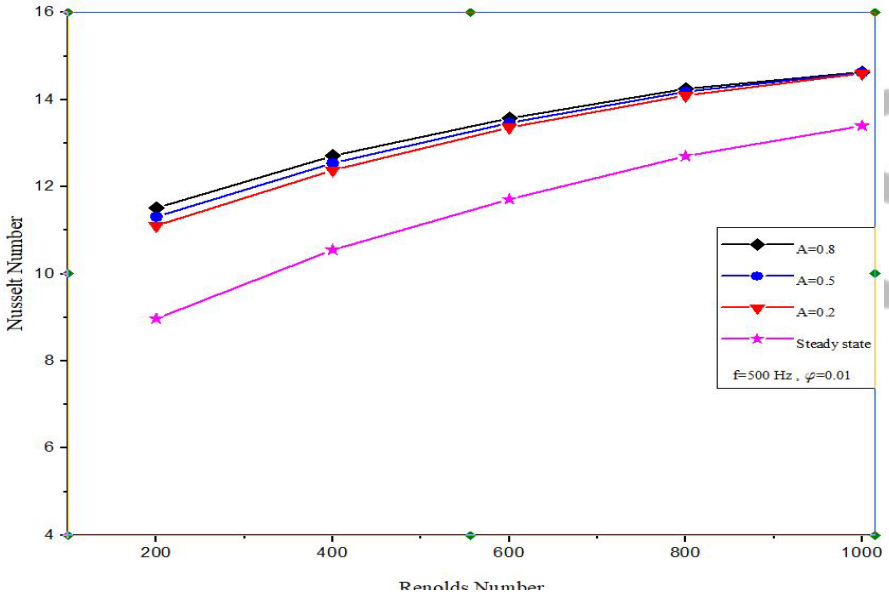

Figure 5c: Comparison of Nu values at various amplitudes and a frequency of 300Hz with steady state

The effect of pulsating frequency on the heat transfer can be explained by the additional heat transfer enhancement which can be attributed to the supplementary mixing effect due to increase in flow unsteadiness which is proportional to the flows Womersley's number (Wo). For a low value of Wo (1 or less), it means the frequency of pulsations is sufficiently low that a parabolic velocity profile has time to develop in a complete cycle, and the flow will be very nearly in phase with the pressure gradient, therefore the flow properties is similar to that of steady state condition. When Wo is large (10 or more), it means the frequency of pulsations is sufficiently large that the velocity profile is relatively flat or plug-like, and the mean flow lags the pressure gradient by about 90 degrees [37], this causes hydrodynamic and thermal boundary layer thinning that has a significant effect on heat transfer [26].
This can be observed in figure 6 that at a constant amplitude of 0.2 for a frequency of 100hz which correspond to a Wo of 3.4, there is a small increase in nusselt number values when compared to that of steady state which also increases with increase in Reynolds number. While for higher value of pulsating frequency of 300hz and 500hz which corresponds to Wo of 5.9 and 7.6, there is a larger increase in nusselt number value when compare to steady state condition due to higher mixing effect as a result of unsteadiness

caused by the pulsating frequency.

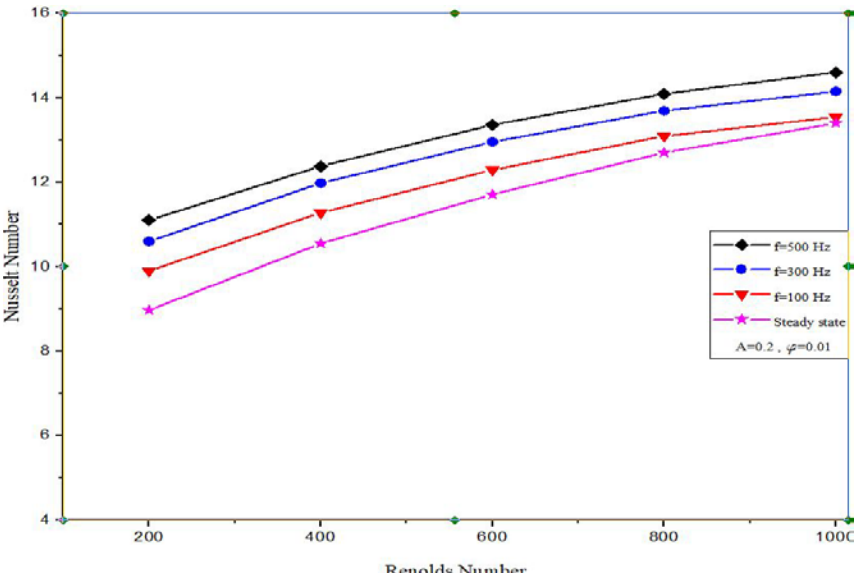

Figure 6: Comparison of Nu values at various frequencies and an amplitude of 0.2 with steady state

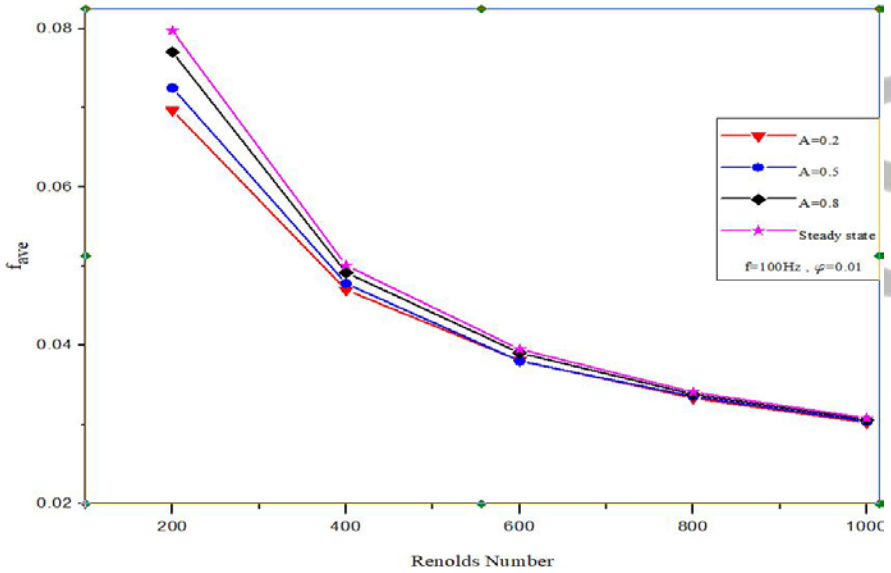

Figure 7: Comparison of f_{ave}values at various Amplitudes and a frequency of 100Hz with steady state

The average friction factor for different amplitude and Reynolds number is presented in Figure 7. The average friction factor is marginally lower for unsteady case when compared to steady condition, which shows that athat significant thermal enhancement can be achieved through pulsating flow with a decrease in pressure drop. It is also observed that averagefriction factor value is higher in low Re region because at this region, the flow is more viscous in nature causing high pressure drop which leads to the enrichment in the friction factor. This implies that flow resistance decreases with higher flow velocity and lower pressure drop.

5 Conclusion

This study examinesnumerically the effect of Al_2O_3–water based nanofluids on heattransfer in an interrupted microchannel heat sink with rectangular rib under pulsating inlet flow conditionsusing the two-phasemixture model approach.The effects of pulsating amplitude and frequency on the average Nusselt number are investigated. At the end of the investigation, the following conclusions are

arrived.

- Pulsating inlet flow condition lead to asignificant increase in rate of heat transfer with a marginal reduction in average friction factor compared with the steady condition.
- There is an increase in Nusselt number wheneverpulsating amplitude is increased. This is due to enhanced mixing within the flow domain; however, the effect is suppressed at higher Reynolds number.
- A higer heat transfer enhancement is observed with increase in pulsating frequency compared withincrreasing pulsation amplitude.

References

[1] D. B. Tuckerman and R. F. W. Pease, High-Performance Heat Sinking for VLSI, IEEE: Electron Device Lett.,vol. EDL-2, pp. 126–129, 1981
[2] X. F. Peng and G. P. Peterson, The Effect of Thermofluid and Geometrical Parameters on Convection of LiquidsThrough Rectangular Microchannels, Int. J. Heat Mass Transfer, vol. 38, pp. 755–758, 1995
[3] T. M. Harms, M. J. Kazmierczak, and F. M. Gerner, Developing Convective Heat Transfer in Deep RectangularMicrochannel, Int. J. Heat Fluid Flow, vol. 20, pp. 149–157, 1999.
[4] Qu, W., &Mudawar, I. (2002b). Experimental and numerical study of pressure drop and heat transfer in a single-phase micro-channel heat sink.*International Journal of Heat and Mass Transfer, 45*(12), 2549-2565.
[5] Ambatipudi, K. K., & Rahman, M. M. (2000). Analysis of Conjugate Heat Transfer in Microchannel Heat Sinks. *Numerical Heat Transfer, Part A:Aplications, 37*(7), 711-731.
[6] Fedorov, A. G., &Viskanta, R. (2000). Three-dimensional conjugate heat transfer in the microchannel heat sink for electronic packaging. *Internatioal Journal of Heat and Mass Transfer, 43*(3), 399-415.
[7] Zhao, C. Y., & Lu, T. J. (2002). Analysis of microchannel heat sinks for electronicscooling. *International Journal of Heat and Mass Transfer, 45*(24), 4857-4869.
[8] Qu, W., &Mudawar, I. (2002a). Analysis of three-dimensional heat transfer in microchannel heat sinks. *Iternational Journal of Heat and Mass Transfer, 45*(19), 3973-3985.
[9] Gamrat, G., Favre-Marinet, M., &Asendrych, D. (2005). Conduction and entrance effects on laminar liquid flow and heat transfer in rectangular microchannels. *International Journal of Heat and Mass Transfer, 48*(14), 2943-2954
[10] Svino, J. M., & Siegel, R. (1946). Laminar forced convection in rectangular channels with unequal heat addition on adjacent sides. *International Journal of Heat and Mass Transfer*, 16, 733–741
[11] Hong, Z.-C., Zhen, C.-E., & Yang, C.-Y. (2008). Fluid Dynamics and Heat Transfer Analysis of Three-Dimensional Microchannel Flows with Microstructures. *Numerical Heat Transfer, Part A: Applications, 54*(3), 293-314.
[12] Hung, T. C., Huang, Y. X., & Yan, W. M. (2013). Thermal performance analysis of porous-microchannel heat sinks with different configuration design, *International Journal of Heat and Mass Transfer*, 66, 235-243
[13] J.L. Xu, Y.H. Gan, D.C. Zhang, Microscale heat transfer enhancement using thermal boundary layer redeveloping concept, Int. J. Heat Mass Transfe-. r 48 (2005) 1662e1674.
[14] Y.J. Cheng, Numerical simulation of stacked microchannel heat sink with mixing-enhanced passive structure, Int. Commun. Heat Mass Transf. 34 (2 007) 295e303
[15] A.J. Foong, N. Ramesh, Laminar convective heat transfer in a microchannel with internal longitudinal fins, Int. J. Therm. Sci. 48 (2009) 1908e1913.
[16] L. Chai, G.D. Xia, M.Z. Zhou, Numerical simulation of fluid flow and heat transfer in a microchannel heat sink with offset fan-shaped reentrant cavities in sidewall, Int. Commun.Heat Mass Transf. 38 (2011) 577e584.
[17] G.D. Xia, L. Chai, M.Z. Zhou, Effects of structural parameters on fluid flow and heat transfer in a microchannel with aligned fan-shaped reentrant cavities, Int. J. Therm. Sci. 50 (2011) 411e419.
[18] G.D. Xia, L. Chai, H.Y. Wang, Optimum thermal design of microchannel heat sink with triangular reentrant cavities, Appl. Therm. Eng. 31 (2011) 1208e1219
[19] L. Chai, G.D. Xia, M. Zhou, J. Li, J. Qi, Optimum thermal design of interrupted microchannel heat sink with rectangular ribs in the transverse microchambers, Appl ThermEng 51 (2013) 880–889.
[20] Ho, C. J., & Chen, W. C. (2013). An experimental study in thermal performance of Al2O3/water nanofluid ina minichannel heat sink. *Applied Thermal Engineering*, 50, 516-522.
[21] Ho, C. J., Liu, W. K., Chang. Y. S., & Lin, C. C. (2010). Natural convection heat transferof alumina-water nanofluid in vertical square enclosure: An experimental study. *International Journal of Thermal Sciences,* 49(8), 1345-1353.
[22] Wang, G., Niu, D., Xie, F., Wang, Y., Zhao, X., & Ding, G. (2015). Experimental andnumerical investigations of a microchannel heat sink (MCHS) with micro-scale ribs and grooves for chipcooling. *Applied Thermal Engineering*, 85, 61-74.
[23] Abbasi, Y., Shirani, A. S., &Asgarian, S. (2015). Two-phase mixture simulation ofAl2O3/water nanofluid heat transfer in a non-uniform heat addition test section.*Progress in Nuclear Energy,* 83, 356-364.
[24] Lotfi, R., Saboohi, Y., & Rashidi, A. M. (2010). Numerical study of forced convective heat transfer of Nanofluids: Comparison of different approaches. *International Communications in Heat and Mass Transfer*, 37, 74-78.
[25] Kalteh, M., Abbassi, A., Saffar-Avval, M., Frijns, A., Darhuber, A., &Harting, J. (2012).Experimental and numerical investigation of nanofluid forced convection insidea wide microchannel heat sink. *Applied Thermal Engineering*, 36 (0), 260-268.
[26] Nandi, T. K., & Chattopadhyay, H. (2014). Numerical investigations of developing flowand heat transfer in raccoon type microchannels under inlet

pulsation,*International Communications in Heat and Mass Transfer*, 56, 37-41, 2014
[27] Akdag, U., Akcay, S. and Demiral, D. (2014) 'Heat transferenhancement with laminar pulsating nanofluid flow in a wavychannel', *Int. Commun.Heat Mass Transfer*, December,Vol. 59, pp.17–23.
[28] Akdag, U., Akcay, S. and Demiral, D.(2017) 'Heat transfer enhancement with nanofluids under laminar pulsating flow in atrapezoidal-corrugated channel', *Progress in Computational Fluid Dynamics*, Vol. 17, No. 5,pp.302–312.
[29] K. Narrein, S. Sivasankaran& P. Ganesan (2016): Numerical investigation oftwo-phase laminar pulsating nanofluid flow in a helical microchannel, Numerical Heat Transfer,Part A: Applications
[30] Fluent 18.3. FLUENT Theory Guide, Fluent, Inc., Lebanon, NH. 03766, USA, 2017.
[31] A. Mahdy, Nuclear Engineering and Design,249 (2012) 248-255.
[32] R.L. Hamilton, O.K. Crosser, Thermal conductivity of heterogeneous twocomponent systems, I EC Fundam. 1 (1962) 187e191.
[33] H.C. Brinkman, The viscosity of concentrated suspensions and solutions, J. Chem. Phys. 20 (1952) 571e581
[34] H.S. Kwak, H. Kin, M.H. Jae, S. Tae-Ho, Thermal control of electroosmotic flow in a microchannel through temperature-dependent properties, J. Colloid Interface Sci. 335 (2009) 123e129.
[35] C.J. Glassbrenner, G.A. Slack, Thermal conductivity of silicon and germanium from 3K to the melting point, Phys. Rev. 134 (1964) A1058eA1069.
[36] Wen, D., & Ding, Y. (2004). Experimental investigation into convective heat transfer ofnanofluids at the entrance region under laminar flow conditions. *InternationalJournal of Heat and Mass Transfer*, 47, 5181-5188
[37] Wikipedia. (2020). Womersley number. [online] Available at: https://en.wikipedia.org/wiki/Womersley_number [Accessed 4 Jun. 2020].